Journal of the American Heart Association

ORIGINAL RESEARCH

Cardiomyocyte Reduction of Hybrid/Complex N-Glycosylation in the Adult Causes Heart Failure With Reduced Ejection Fraction in the Absence of Cellular Remodeling

Anthony M. Young, MSc; John A. Miller, PhD; Andrew R. Ednie, PhD; Eric S. Bennett, PhD

BACKGROUND: Heart failure (HF) presents a massive burden to health care with a complex pathophysiology that results in HF with reduced left ventricle ejection fraction (EF) or HF with preserved EF. It has been shown that relatively modest changes in protein glycosylation, an essential posttranslational modification, are associated with clinical presentations of HF. We and others previously showed that such aberrant protein glycosylation in animal models can lead to HF.

METHODS AND RESULTS: We develop and characterize a novel, tamoxifen-inducible, cardiomyocyte *Mgat1* knockout mouse strain, achieved through deletion of *Mgat1*, alpha-1,3-mannosyl-glycoproten 2-beta-N-acetylglucosaminyltransferase, which encodes N-acetylglucosaminyltransferase I. We investigate the role of hybrid/complex N-glycosylation in adult HFrEF pathogenesis at the ion channel, cardiomyocyte, tissue, and gross cardiac level. The data demonstrate successful reduction of N-acetylglucosaminyltransferase I activity and confirm that hybrid/complex N-glycans modulate gating of cardiomyocyte voltage-gated calcium channels. A longitudinal study shows that the tamoxifen-inducible, cardiomyocyte *Mgat1* knockout mice present with significantly reduced systolic function by 28 days post induction that progresses into HFrEF by 8 weeks post induction, without significant ventricular dilation or hypertrophy. Further, there was minimal, if any, physiologic or pathophysiologic cardiomyocyte electromechanical remodeling or fibrosis observed before (10–21 days post induction) or after (90–130 days post induction) HFrEF development.

CONCLUSIONS: The tamoxifen-inducible, cardiomyocyte *Mgat1* knockout mouse strain created and characterized here provides a model to describe novel mechanisms and causes responsible for HFrEF onset in the adult, likely occurring primarily through tissue-level reductions in electromechanical activity in the absence of (or at least before) cardiomyocyte remodeling and fibrosis.

Key Words: EC coupling ■ echocardiography ■ heart failure ■ N-glycosylation ■ voltage-gated ion channels

One of the primary functions of cardiomyocytes, electromechanical activity, is achieved through the highly tuned activity of voltage-gated ion channels (VGICs), which activate Ca^{2+}-driven excitation–contraction (EC) coupling and lead to myocyte contraction and relaxation. This cellular electromechanical signaling must be conducted cell to cell across the myocardium to allow for the coordinated contraction of the heart and, thereby, the optimal pumping of blood. When this cellular process is disrupted or stressed,

Correspondence to: Eric S. Bennett, Department of Neuroscience, Cell Biology & Physiology, Wright State University, 143 Biological Sciences II, 3640 Colonel Glenn Hwy, Dayton, OH 45435. Email: eric.bennett@wright.edu

Supplemental Material is available at https://www.ahajournals.org/doi/suppl/10.1161/JAHA.124.036626

This article was sent to Julie K. Freed, MD, PhD, Associate Editor, for review by expert referees, editorial decision, and final disposition.

For Sources of Funding and Disclosures, see page 13.

JAHA is available at: www.ahajournals.org/journal/jaha

RESEARCH PERSPECTIVE

What Is New?

- This work uses a novel model to demonstrate that a postdevelopmental reduction in hybrid/complex N-glycosylation leads to heart failure with reduced ejection fraction without significant cardiomyocyte remodeling or fibrosis.
- The data show an acute effect of aberrant N-glycosylation on voltage-gated Ca^{2+} channels, but this is not sufficient alone to disrupt individual cardiomyocyte Ca^{2+} transients or contractility.
- These findings suggest that N-glycosylation plays a significant role in tissue-level cardiac electromechanical function.

What Question Should Be Addressed Next?

- What role do cardiomyocyte N-glycans play at the intercalated discs to establish normal electromechanical coupling at the tissue level?
- What other pathophysiologic processes underlie the development of heart failure with reduced ejection fraction in the absence of cardiomyocyte remodeling and fibrosis?

Nonstandard Abbreviations and Acronyms

cMgat1KO	constitutive cardiomyocyte *Mgat1* knockout
DCM	dilated cardiomyopathy
DPI	days post induction
FS	fractional shortening
GNL	*Galanthus nivalis* lectin
HFrEF	heart failure with reduced ejection fraction
ICD	intercalated disc
iMgat1KO	tamoxifen-inducible, cardiomyocyte *Mgat1* knockout
TCre	tamoxifen-inducible Cre recombinase
VGIC	voltage-gated ion channel

tissue-level arrythmias and aberrant contraction can develop, often leading to cardiomyopathy that can deteriorate into heart failure (HF).

With about 64 million people affected by HF worldwide, it is critical to understand the mechanisms that can lead to HF with the pursuit of increasing the current repertoire of preventative and treatment options for patients.[1] HF is a clinically defined diagnosis that can generally be classified using left ventricular (LV) ejection fraction (EF) as HF with reduced EF (HFrEF, EF<40%) or preserved EF (EF>50%).[2] Different molecular and cellular changes underlie these distinct disease progressions of HF.[3] The proposed pathophysiologic framework of HFrEF in many models is that depressed calcium-dependent cardiomyocyte contractility is associated with the gross systolic dysfunction of the cardiac tissue.[4–7] As HF progresses, cardiomyocytes often undergo electrophysiologic remodeling generally associated with action potential (AP) prolongation likely due to reduced voltage-gated K^+ channel (K_v) activity, generating a proarrhythmic state[8–14] as well as increased fibrosis that contributes to aberrant conduction.[15]

N-linked glycosylation is a common co–/post-translational modification in which saccharides are sequentially bound to asparagine side chains in the extracellular domain of transmembrane proteins, a dynamic process requiring the activity of hundreds of regulated gene products.[16,17] The diverse glycans that result modify the biochemical properties of glycoproteins and are necessary for cellular physiology, including protein stabilization, receptor recognition, and cellular motility.[18–20] Inherited mutations in glycan synthesis or processing can lead to a heterogenous family of diseases known as congenital disorders of glycosylation, which frequently can present with cardiomyopathies and lead to HFrEF.[21–24] Additionally, gene expression studies in humans with idiopathic dilated cardiomyopathy (DCM) have shown altered expression of glycosylation-related genes,[25,26] including alpha-1,3-mannosyl-glycoproten 2-beta-N-acetlyglucosaminyltransferase (*Mgat1*).[27] These findings suggest that there could be an underlying pathophysiologic connection between HFrEF and aberrant N-glycosylation.

Our laboratory and others have shown that the addition of extracellularly facing N- and O-glycans to VGICs can directly affect neuronal, skeletal muscle, and cardiac VGIC gating and contribute to progressive cardiac dysfunction. Notably, the normal glycosylation within cardiomyocytes can be crucial for the proper function of voltage-gated Na^+ channels (Na_v), calcium channels (Ca_v), and some K_v isoforms.[28–35] Sialic acids, which terminate hybrid/complex branches of N-glycans and O-glycans, play a pivotal role in the biophysical properties of these channels, and aberrant sialylation leads to atypical voltage-gating and pressure-induced DCM and HFrEF in mouse models.[31,32,36] Altered sialylation has also been associated with the clinical presentation of patients with Brugada syndrome.[37] Tangentially, it was shown that cardiomyocyte-specific Ca_v activity and expression is regulated by intracellular O-GlcNAcylation and when chronically reduced leads to HFrEF in mouse models.[38,39]

N-acetylglucosaminyltransferase I (GlcNAcT1), encoded by *Mgat1*, is responsible for initiating the formation of hybrid/complex N-glycans from simple and trimmed

oligomannosidic N-glycans.[40] Our previous work established a mouse model that employed a cardiomyocyte MYH6 (myosin heavy chain 6) promoter-driven, cre-recombinase knockout of *Mgat1* constitutively, starting in the embryonic stage.[33,34,41] These constitutive cardiomyocyte *Mgat1* knockout mice (cMgat1KO) die prematurely with significantly dilated, fibrotic hearts with gross dysfunction. The diseased cMgat1KO cardiomyocytes demonstrated altered electromechanical function, including significant depolarizing shifts in Ca_V gating, likely due to the direct effect of reduced complex N-glycans and thereby reduced channel sialylation. Further, there was marked impairment of cardiomyocyte function at early disease stages that worsened with disease progression resulting from, for example, reduced K_V expression and activity, extended AP duration, and aberrant Ca^{2+} transients and contractility.[33,34] However, because of the coincident progression of cellular and whole heart dysfunction, it was not possible to determine whether the worsening cardiomyocyte functions were responsible for, contributed to, or resulted from HF onset.

Here, our working hypothesis was that the altered gating of VGICs due to the loss of GlcNAcT1 was sufficient to directly initiate progressive cardiomyocyte electromechanical dysfunction, such as extended AP duration and aberrant myocyte EC coupling, which began before and contribute to the development of DCM and HFrEF. To test this hypothesis, we developed and characterized a novel, cardiomyocyte-specific, tamoxifen-inducible *Mgat1* knockout mouse model (iMgat1KO) to enable us to more closely investigate the timeline of disease progression and the contributions of cardiomyocyte remodeling to disease progression (or not) following the reduction in hybrid/complex N-glycosylation in adult mice. In addition, adult deletion of *Mgat1* removes any complications due to pre- and postnatal developmental changes that occur in the murine heart, including expression of different K_V isoforms[14,42] and altered glycosylation.[29,43] Thus, here we study cardiac function across time after the loss of GlcNAcT1 in adult cardiomyocytes, at the VGIC, cardiomyocyte, tissue, and gross cardiac levels. The data refute our working hypothesis, indicating instead that reduced complex/hybrid N-glycosylation in the adult is responsible for HFrEF onset, occurring primarily through tissue-level reductions in electromechanical activity in the absence of (or at least before) cardiomyocyte remodeling and fibrosis.

METHODS

Transparency and Openness Promotion Statement

The authors declare that all data and materials used here are available upon request by contacting the corresponding author, Eric Bennett at eric.bennett@wright.edu.

Animal Care and Ethical Consideration

All handling and care of mice adhered to the National Institutes of Health *Guide for the Care and Use of Laboratory Animals* and were approved by the Wright State University Institutional Animal Care and Use Committee (Animal Use Protocol 1229). For in vivo echocardiographic studies, the animals were anesthetized with ~2.0% to 3.0% isoflurane/O_2 before and throughout the protocol. Each mouse was euthanized under deep anesthesia (5.0% isoflurane/O_2) via thoracotomy and excision of the heart to obtain samples for biochemical and cellular studies. We used the Animal Research: Reporting of In Vivo Experiments checklist when writing our report to ensure we met appropriate reporting guidelines for preclinical animal studies.[44]

Generation of the iMgat1KO and Animal Use

To create the iMgat1KO, mice homozygous for LoxP sites flanking the only coding exon for *Mgat1,* as used by Marth[45] and us previously[33,34] (commercially available from the Jackson Laboratory, 006891), were crossed with mice hemizygous for the α-MHC-MerCreMer transgene containing the cardiomyocyte-specific promoter to drive the expression of a downstream tamoxifen-inducible Cre recombinase (Jackson Laboratory, 005657). To achieve deletion of the *Mgat1* after complete cardiac development, male iMgat1KO mice were placed on a regimen of tamoxifen-infused chow (250 mg/kg feed; TD.130855; Envigo) for 28 days starting between 8 and 10 weeks of age. To control for possible detrimental cardiac effects due to α-MHC-MerCreMer expression or tamoxifen treatment,[46,47] age-matched, α-MHC-MerCreMer positive, male mice were used as control mice and treated with the same tamoxifen-infused chow regimen as described (TCre). Groups of 3 littermates from the iMgat1KO or TCre group were housed together during and after the tamoxifen treatments. The original colonies of mice were from Jackson Laboratories and Dr J. Marth, but the mice used here were from colonies maintained at the Wright State University Laboratory Animal Resources Department.

Protein Lysates and Immunoblotting

Sarcolemma-enriched protein lysates were collected from individual hearts in a manner adapted from others' work[48] and previously described.[39] Excised hearts were washed in PBS, and the ventricles were homogenized in a buffer containing (in millimolar; mM): 20 4-(2-hydroxyethyl)-1 piperazineethanesulfonic acid

(HEPES), 250 sucrose, 2 EDTA, 1 $MgCl_2$, pH 7.4 supplemented with 1X Complete Ultra protease inhibitor cocktail (5892970001; Roche), 1X PhosSTOP phosphatase inhibitor tablet (4906845001; Roche, Mannheim, DE), 0.01 calpain inhibitors I and II (A2602 and AA2603; Apex Bio, Houston, TX), and 0.001 thiamet G (13237; Caymen Chemical, Ann Arbor, MI). Debris and nuclei were removed by spinning the lysates at 400*g* for 20 minutes followed by a 45 minutes spin at 33 000*g*. The pellet containing sarcolemma-enriched protein was then resolubilized in (in mM unless noted): 20 HEPES, 150 NaCl, 0.02% (weight to volume, w/v) Na^+ azide, 1 tris(2-carboxyethyl)phosphine, and 0.5% (w/v) amidosulfobentaine supplemented as described and clarified by centrifugation. As previously described, 40 μg of the lysates were used for gel electrophoresis, Western blotting, and immunodetection.[32,33,35] Biotinylated GNL (*Galanthus nivalis* lectin; B-1245; Vector Labs, Newark, CA), which preferentially targets α-1,3 mannose residues,[49] was used to detect high-mannose N-glycans and visualized with NeutrAvidin (31030; Thermo Fisher Scientific, Waltham, MA) as previously described.[33] Immunodetection of the Ca_V α2δ1 subunit was performed using an antibody specific for the Ca_V α2δ1 subunit (ACC-015; Alomone, Jerusalem, Israel) and visualized with a goat antirabbit IgG-horseradish peroxidase (AP307P; MilliporeSigma, Burlington, MA).[33,39] 2,2,2-trichloroethanol was added to the electrophoretic gel to achieve total protein staining to normalize the horseradish peroxidase signals following the immunodetection.[50,51] Analysis of the immunoblot was performed in ImageLab (Bio-Rad Laboratories, Hercules, CA).

Echocardiography

Transthoracic echocardiography measurements were performed on mice under anesthesia with ~2.0% to 3.0% isoflurane/O_2. A Vevo 3100 system (Fujifilm, Tokyo, Japan) was equipped with a 30-MHz transducer to acquire mid-LV parasternal long- and short-axis views as well as parasternal short-axis M-mode recordings as done before.[33] Recordings were acquired and analyzed using VevoLabs (VisualSonics, Toronto, Canada) to determine hemodynamic parameters of the hearts.[33,36] The analysis was completed blindly by someone separate from the one who completed the recordings. Baseline measurements were first obtained in a cohort of iMgat1KO and TCre mice before placing the mice on the 28-day tamoxifen regimen (discussed previously). The first recordings following the treatment were completed 7 days post induction (DPI), after removing the mice from the tamoxifen. These measurements were completed longitudinally on the same cohort of mice through 168 DPI.

Cardiomyocyte Isolation

As described before,[32,35,38,52] ventricular cardiomyocytes were isolated via Langendorff perfusion of iMgat1KO and TCre hearts using 0.6 to 1.0 mg/mL collagenase type II (Worthington Biochemical, Lakewood, NJ) and 0.5 units/mL protease XIV (P5147; Sigma Aldrich, St. Louis, MO). Following digestion of the hearts, the ventricles were removed, and individual ventricular cardiomyocytes were mechanically dispersed. Over the 10 minutes following isolation, the 2,3-butanedione monoxime and Ca^{2+} concentrations were sequentially lowered and raised to 0 and 1.2 mM, respectively. The myocytes were stored for 1 to 6 hours in Hank's balanced salt solution (12350-039; Thermo Fisher Scientific) at room temperature until use. Ventricular cardiomyocytes were isolated from mice at early (10–21 DPI) and late (90–130 DPI) time points after *Mgat1* deletion.

Cardiomyocyte Electrophysiology

Electrophysiologic measurements of the isolated cardiomyocytes were completed at room temperature using whole-cell patch techniques. Ca_V activity was measured as done previously.[33,38] Ventricular myocytes isolated between 19 and 21 DPI were perfused with a buffer containing (in mM): 10 HEPES, 10 glucose, 136 NaCl, 1.0 $CaCl_2$, 1.0 $MgCl_2$, 4.0 tetraethyl ammonium chloride (to block K^+ channels), and 0.02 tetrodotoxin (to block Na^+ channels), pH 7.4. The patching pipettes contained an intracellular solution of 10 HEPES, 10 EGTA, 5 glucose, 135 CsCl, and 4.0 Mg^{2+} adenosine 5′-triphosphate, pH 7.2. To measure voltage-sensitive Ca^{2+} currents, the myocytes were clamped at –70 mV and underwent a series of 1.2-second depolarizations ranging from –40 mV to 30 mV in 10 mV increments, each separated by 15 s intervals. Before each depolarization, the myocytes were depolarized with a 50 ms prepulse to –40 mV to inactivate Na_V channels.[33] The reversal potential was empirically determined for each cell and used to calculate the driving force at each depolarization to calculate the conductance using each maximum negative current. This voltage–conductance relationship was fit to a Boltzmann function to determine activation-gating parameters.[33,35,38,39] To measure voltage-dependent inactivation Ca_V activity, the myocytes were held at –70 mV and underwent conditioning pulses beginning at –50 mV to 10 mV in 10 mV increments for 400 ms before the cells were depolarized to 20 mV for 400 ms. Each incremental voltage step was separated by a delay of 15 seconds. Each maximum negative current was normalized to the maximum value from the first step to –20 mV and fit to a Boltzmann function to determine inactivation gating parameters.[33,35,38,39] APs and potassium currents (I_K) were recorded from LV apex cardiomyocytes and

analyzed as previously described.[32,34,35] An extracellular perfusion solution was used to record I_{K+}, which consisted of (in mM) 10 HEPES, 10 glucose, 136 NaCl, 0.5 $CaCl_2$, 1.0 $MgCl_2$, 0.25 $CdCl_2$ (to block Ca^{2+} currents), 5.4 KCl, and 0.02 tetrodotoxin, pH 7.4. Patch pipettes were filled with an intracellular recording solution of (in mM): 10 HEPES, 10 EGTA, 1.0 Mg^{2+} triphosphate, 5.0 glucose, 135 KCl, and 4.0 K_2 adenosine 5′-triphosphate, pH 7.2. The same pulse protocols and analysis as described previously were used in this study.[32,34,35]

Cardiomyocyte Calcium Transients and Contractility

Both whole-cell Ca^{2+} transients and contractility of isolated ventricular myocytes were recorded at room temperature as previously described.[33,38] For both sets of measurements, cardiomyocytes were perfused in a recording chamber (SPC Microscope Chamber System; IonOptix, Westwood, MA) with Hank's balanced salt solution with 10 mM of HEPES. The cardiomyocytes were allowed to settle onto a glass slide and stimulated with 20 mV, 4 ms pulses at 0.5Hz (MyoPacer; IonOptix). Before the Ca^{2+} transient measurements, the cells were loaded with 1 μM Fura-8 for 20 minutes and then washed with Hank's balanced salt solution. Fluorescence signals were ratiometrically recorded under 354 nm and 415 nm excitation and the emissions were filtered and detected with a photometry system (PTI RatioMaster; Horiba Scientific, Edison, NJ) and recorded using FelixGX (PTI; Horiba Scientific). For contractility measurements, cardiomyocytes underwent the same protocol without the loading of Fura-8. Contractions were recorded by edge detection at 250 Hz with IonWizard 7.4 (IonOptix) under the same stimulation described previously. The IonWizard software was used to analyze both the Ca^{2+} transients and myocyte contractility.

Histology and Fibrosis Quantification

Excised hearts were washed in PBS (Fisher Scientific) twice following excision from iMgat1KO and TCre mice under deep anesthesia (5.0% isoflurane/O_2). The hearts were fixed in 4% paraformaldehyde for 1 hour at room temperature and then overnight at 4 °C. The hearts were then placed in PBS with 10% ethanol and shipped to AML Laboratories (St. Augustine, FL) where they were embedded in paraffin and sectioned at 5 μm along a midventricular coronal plane. To quantify the amount of fibrosis in the hearts, sections were deparaffinized in xylene, rehydrated, and stained with picrosirius red solution (SRS-IFU; ScyTek, West Logan, UT) for 60 minutes. The sections were then washed in acetic acid, dehydrated in absolute alcohol, and mounted. The stained sections were imaged at 1X under brightfield illumination and analyzed in FIJI.[53] To quantify the amount of positively stained collagen (red) in the ventricles, a region of interest was chosen to include the ventricular tissue, and the amount of collagen was quantified as a percentage of ventricular area using a deconvolution method as described by others.[54]

Statistical Analysis

Statistical analysis and preparation of graphs were performed in SigmaPlot (Grafiti; Palo Alto, CA), RStudio (RStudio, PBC; Boston, MA), and Prism (GraphPad; La Jolla, CA). Figures were edited and formatted with Adobe Illustrator (Adobe Inc; San Jose, CA). All data are presented as the mean±SEM unless otherwise specified in the figure legend. To determine if/when EF or fractional shortening (FS) significantly differed between the control and iMgat1KO mice, 2-way repeated measures ANOVA and Sidak post hoc tests were performed. A 2-way ANOVA of medians and corresponding post hoc tests (WRS2 R-package 'med2way()' and 'mcp2a()' functions)[55] were performed on the quantified LV fibrosis over time. Otherwise, significant differences were determined with an unpaired, 2-tailed Student's *t* test or Mann–Whitney rank-sum test based on the normality of the distribution of data determined using a Shapiro–Wilk test with a critical *P* value of 0.05. Only *P* values <0.05 are shown in the figures. The number of animals used is indicated by "N," and the number of cells used is indicated by "n."

RESULTS

Induced *Mgat1* Deletion in Adult Cardiomyocytes Leads to Reduced Hybrid/Complex N-Glycosylation and Heart Failure

To establish that the induction protocol successfully reduced GlcNAcT1 activity in cardiomyocytes, a large shift in the extent of hybrid/complex N-glycosylation toward high mannose structures was demonstrated by the significant increase in GNL staining of Western blots of cardiac protein from iMgat1KO lysates compared with control (TCre) lysates (Figure 1A and 1B). Because GNL specifically binds to uncapped, α-1,3 mannose residues,[49] the observed 3.4-fold increase in GNL staining in the iMgat1KO lysates (Figure 1A and 1B) suggests a successful and significant reduction in GlcNAcT1 activity in the iMgat1KO hearts. In addition, this immunoblotting pattern is comparable to the pattern of staining previously observed in the cMgat1KO mouse model,[33] suggesting that there is a similar reduction in the extent of hybrid/complex N-glycosylation in the constitutive (cMgat1KO) and inducible (iMgat1KO) models.

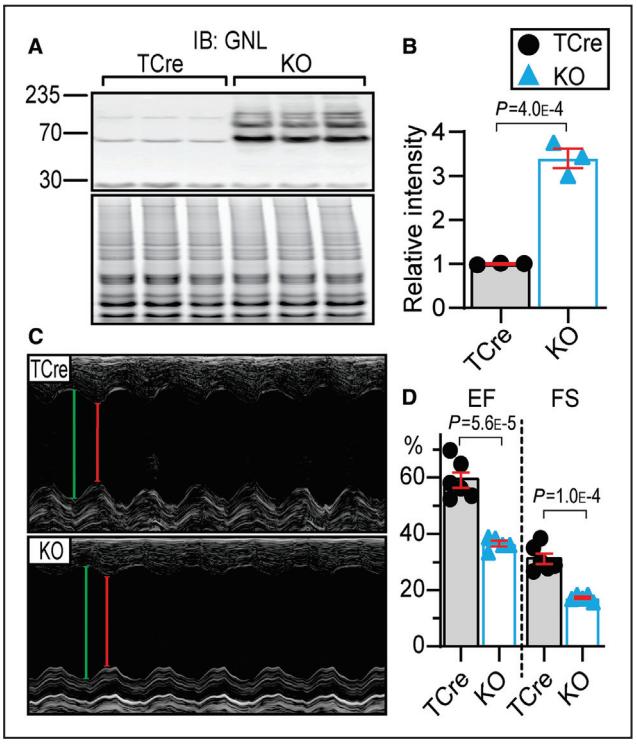

Figure 1. Diminished Mgat1 expression and GlcNAcT1 activity leads to reduced ejection fraction by 112 days post induction.
Successful reduction of Mgat1 expression led to significant reduction in EF and FS at 112 DPI. **A**, Reduced hybrid/complex N-glycosylation was demonstrated with a Western blot of cardiac protein lysates challenged with GNL (immunoblot, IB: GNL), a lectin with preferential binding toward α-1,3 mannose terminated glycans, at 25 DPI. When compared with the controls (TCre), the cardiac lysates from the iMgat1KO had a much higher affinity for GNL, indicating the increased presence of uncapped mannoses. Molecular weights are shown on the left in kDa. N=3. **B**, Quantification of GNL Western blots. The optical density of each lane was normalized to total protein levels (**A**, bottom) and showed a 3.4-fold increase in GNL staining for iMgat1KO lysates (blue, triangles) relative to controls (black, circles), N=3. **C**, Representative short-axis M-mode scans taken from control TCre (top) and KO (bottom) mice at 112 DPI. Green arrows: end systolic left ventricular internal diameter; Red arrows: end diastolic left ventricular internal diameter. **D**, At 112 DPI, the iMgat1KO mice had significantly reduced EF and FS compared with controls (EF: 59.1±2.8% vs 36.6±1.0%; FS: 31.1±1.9% vs 17.1±0.5% (mean±SEM); N=6/5 animals; TCre/iMgat1KO). Unpaired, 2-tailed Student's *t* test. DPI indicates days post induction; EF, ejection fraction; FS, fractional shortening; GNL, *Galanthus nivalis* lectin; KO, knockout; and TCre, tamoxifen-inducible Cre recombinase.

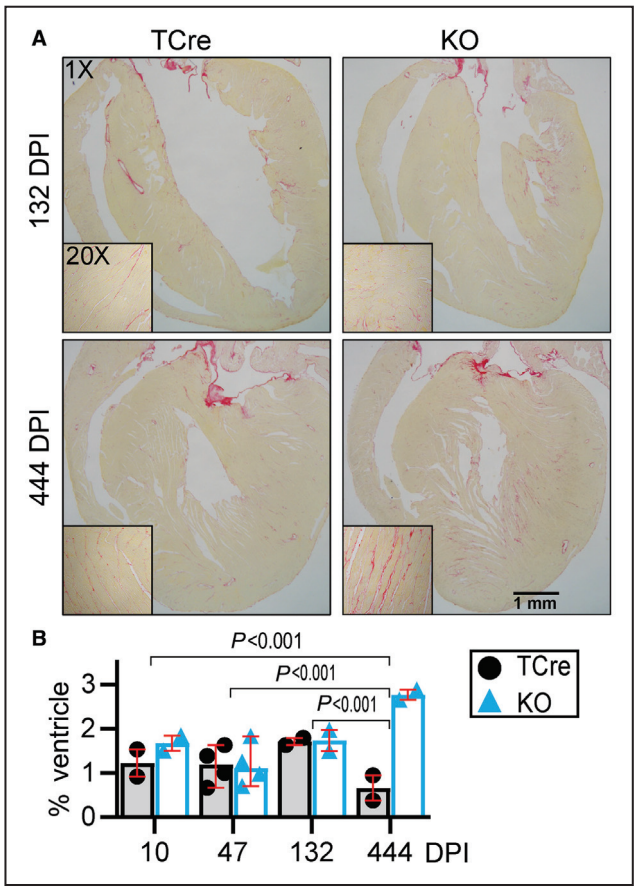

Figure 2. Cardiac fibrosis does not precede the onset of heart failure with reduced ejection fraction.
PSR staining demonstrated no significant increase in fibrosis (collagen deposition, red) in the iMgat1KO ventricles through 132 DPI. **A**, Top panels: representative examples of control (TCre; left) and iMgat1KO (right) hearts at 132 DPI. Bottom panels: Representative examples of control (TCre; left) and iMgat1KO (right) hearts at 444 DPI in the knockouts, well after the onset of HFrEF. Inserts: 20× magnification. (Scale bar=1000 μm, 1× magnification). **B**, Quantification of extracellular collagen deposition over time, post induction. Data shown represent the percent of ventricular tissue positively stained with PSR. The iMgat1KOs showed a significantly greater increase in extracellular collagen from each time point to 444 DPI compared with controls. Medians with 95% CIs are shown. N=2 except at 47 dpi. N=4; 2-way ANOVA of medians and post hoc tests. DPI indicates days post induction; HFrEF, heart failure with reduced ejection fraction; iMgat1KO, tamoxifen-inducible, cardiomyocyte *Mgat1* knockout; KO, knockout; PSR, picrosirius red; and TCre, tamoxifen-inducible Cre recombinase.

To determine the impact of reduced complex N-glycosylation on gross cardiac function, echocardiograms of iMgat1KO and control (TCre) mice were performed at 112 days DPI, a time point (16 weeks) consistent with our previous studies on the cMgat1KO model (Figure 1C).[33] At this time point, *Mgat1* deletion led to considerably reduced systolic function with an LVEF of just 37% and FS of 17% compared with 59% EF and 31% FS in the control group ($P<0.001$) (Figure 1D). These findings suggest that the induced, cardiomyocyte-specific GlcNAcT1 knockout in adult mice significantly diminished cardiac function, consistent with HFrEF, within 16 weeks post-*Mgat1* deletion.

Myocardial Fibrosis Is Not Increased in the iMgat1KO Failing Hearts

The rhythmic beating of the heart is dependent on the synchronous communication between cardiomyocytes established through the conduction of APs across

the myocardium. The slowing of conduction velocity is typical of and contributes to the arrhythmogenicity observed in patients with HF.[15] The electrical conduction across the myocardium proceeds from one cardiomyocyte to the next across gap junctions embedded in the intercalated discs (ICDs)—ICDs electromechanically couple adjacent individual cells.[56] One mechanism that could lead to the disruption of ICDs is through fibrotic remodeling of the extracellular matrix and is common to cardiac injuries that lead to HFrEF.[15,57] To determine if the observed EF reduction in the iMgat1KO mice is secondary to, or coincident with fibrosis, picrosirius red staining was quantified (Figure 2A). Unlike the overt fibrosis previously observed in the cMgat1KO model by 16 weeks of age,[33] the visual and analyzed data here strongly suggest that there was no significant increase in ventricular extracellular collagen deposition in the iMgat1KO from 10 DPI through 132 DPI, well beyond HFrEF onset (Figure 2B). Visual assessment demonstrated a lack of increased fibrosis at all time points except at 444 DPI, at which point there was a clear increase in ventricular fibrosis in the iMgat1KO hearts relative to the controls and earlier time points (Figure 2A).

Aberrant N-Glycosylation Causes a Depolarizing-Shift in Ca_v Gating

Our laboratory previously showed that Ca_v α2δ1 subunits are direct targets of GlcNAcT1 demonstrated through a decrease in Ca_v α2δ1 subunit molecular weight and loss of GlcNAcT1-dependent N-glycans in cardiac tissue.[33] These glycosylation changes were accompanied by depolarizing shifts in Ca_v gating in isolated cardiomyocytes and a significant reduction in Ca_v α2δ1 protein expression. Thus, similar Western blot analyses of the iMgat1KO versus TCre lysates were performed to test whether the same direct effects on this critically important cardiac VGIC are replicated in the iMgat1KO strain. The observed 22 kDa decrease in molecular weight of the Ca_v α2δ1 subunit in the iMgat1KO lysates indicates a significant reduction in mass with the incomplete N-glycan synthesis associated with the loss of GlcNAcT1 (Figure 3A). Additionally, there was a significant reduction in the total Ca_v α2δ1expression relative to TCre (Figure 3B). Steady state activation and inactivation curves were significantly shifted in iMgat1KO cardiomyocytes with 3.7 mV and 2.4 mV rightward shifts in Ca_v half-activation and half-inactivation potentials ($V_{a,1/2}$, $V_{i,1/2}$) relative to the TCre myocytes (Figure 3D). This reinforces our previous findings that hybrid/complex N-glycans, which are generally terminated with a negatively charged sialic acid, can modulate the voltage-dependence of cardiomyocyte VGIC gating. These experiments were performed on cardiomyocytes isolated at 11 to 21 DPI,

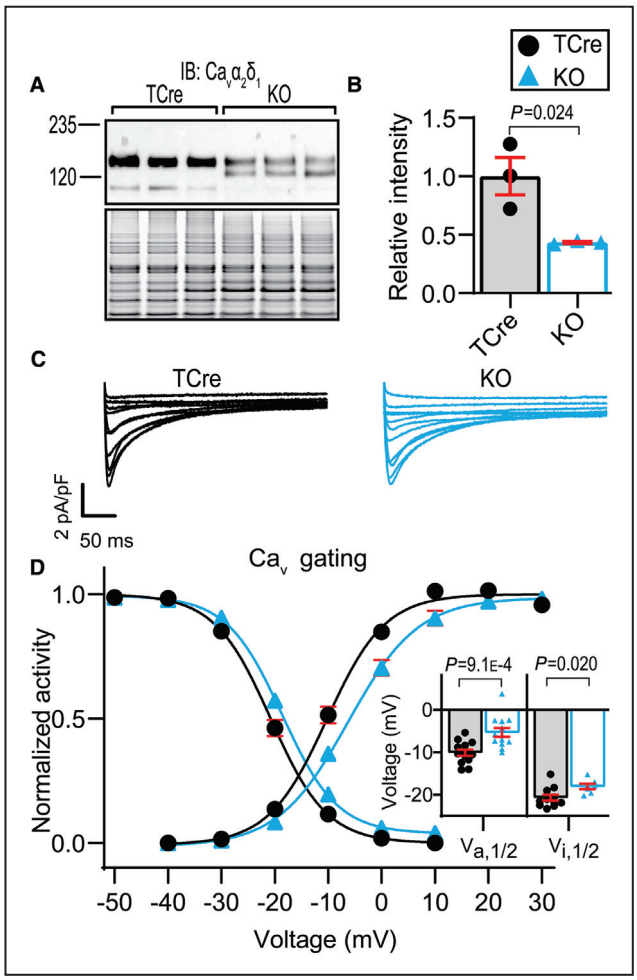

Figure 3. Acute effects of GlcNAcT1 on Ca_v.
GlcNAcT1 directly targets the Ca_v α2δ1 subunit and shifts Ca_v gating at 25 DPI. **A**, Western blot for Ca_v α2δ1 subunit (immunoblot, IB: $Ca_v\alpha2\delta1$) indicated a significant 22 kDa reduction in size in protein lysates from iMgat1KO (KO) hearts relative to controls (TCre) at 25 DPI (mean±SEM: 149±0.3 kDa vs 127±0.1 kDa, $P<0.01$). **B**, Quantification of blots to determine relative expression levels. The optical density of each lane between 120 kDa and ~200 kDa (**A**, top) was normalized to total protein (**A**, bottom), indicating a reduction in Ca_v α2δ1 expression (1.00±0.16 vs 0.43±0.01; N=3). **C**, Representative whole-cell voltage-sensitive Ca^{2+} current traces recorded from control (black) and iMgat1KO (blue) ventricular myocytes. **D**, The Ca_v gating and window current were associated with depolarized shifts in half-activation (Va,1/2; −9.9±0.7 mV vs −6.2±0.6 mV; N=2 animals, n=13 cells) and half-inactivation potentials (Vi,1/2; −19.9±0.6 mV vs −17.5±0.5 mV). N=2/1, n=13/7 control/iMgat1KO). Unpaired, 2-tailed Student's *t* test. Ca_v indicates calcium channels; DPI, days post induction; GlcNAcT1, N-acetylglucosaminyltransferase I; iMgat1KO, tamoxifen-inducible, cardiomyocyte *Mgat1* knockout; KO, knockout; and TCre, tamoxifen-inducible Cre recombinase.

which, along with the evidence that Ca_v complexes are direct targets of GlcNAcT1, are consistent with that shown previously for the cMgat1KO myocytes and support conclusions that Ca_v gating shifts are direct effects of aberrant N-glycosylation.

Heart Failure With Reduced Ejection Fraction Progressively Develops Following the Induced Deletion of *Mgat1*

To better understand the development and progression of the gross, in vivo effects of reduced hybrid/complex N-glycosylation on the heart, echocardiograms were performed on TCre and iMgat1KO mice before and at several time points following induction of *Mgat1* deletion. Baseline measurements were conducted before the mice began the 4-week tamoxifen treatment at 60 days old. There was no difference in mortality between the induced iMgat1KO and controls throughout the 24-week postinduction longitudinal study. The EFs of the iMgat1KO cohort at baseline and for the first 3 weeks after tamoxifen treatment were statistically the same as the control cohort EF over those time points; the TCre cohort EF remained statistically constant throughout the longitudinal study at around 58% (Figure 4A). However, there was a sharp reduction in the mean iMgat1KO EF from 58% to 47% and decrease in FS from 30% to 23% between 21 and 28 DPI (Figure 4A and 4B); again, the TCre cohort did not demonstrate any significant change in systolic function over the same time span. This significant reduction in systolic function of the iMgat1KO cohort relative to baseline EF/FS and time point-matched TCre EF/FS persisted and worsened throughout the entire set of echocardiographic studies (Figure 4A and 4B), down to 33% and 16% for iMgat1KO EF and FS at 168 DPI, respectively, compared with the constant control levels of 58% and 30%. Throughout the experiment, the ventricular wall thickness and lumen diameter did not vary greatly from the controls besides a slight, yet significant, thickening of the diastolic LV anterior wall thickness relative to baseline measurements in the iMgat1KO hearts (Tables S1). These findings indicate that the loss of GlcNAcT1 leads to HFrEF without myocardial dilation or profound hypertrophy. These results motivated the further examination of functional studies on isolated cardiomyocytes before and after the onset of HFrEF, to determine whether and which cellular, disease-related remodeling preceded or followed the onset of reduced systolic function at 28 DPI.

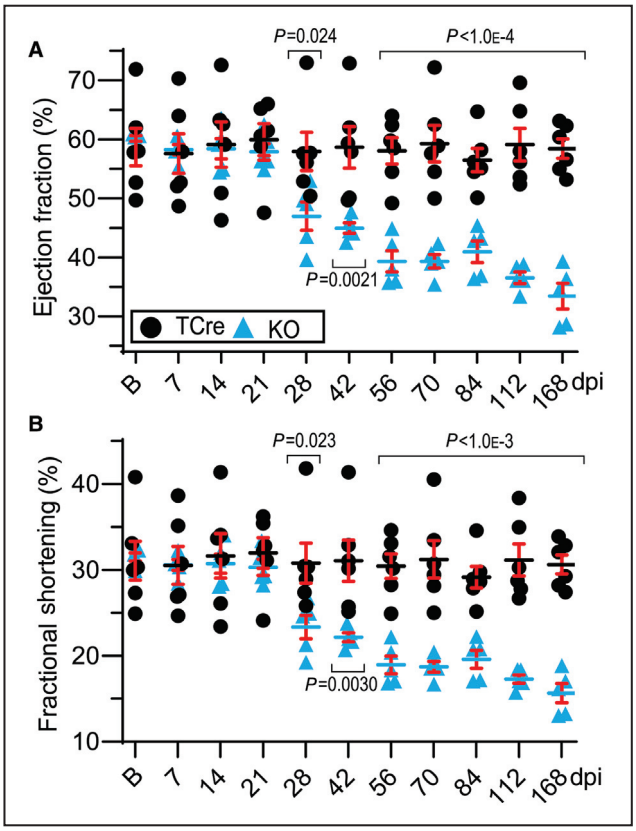

Figure 4. A longitudinal echocardiographic assessment of iMgat1KO cardiac function.
Echocardiograms recorded before tamoxifen treatment ("B" on the *x* axes) through 168 DPI shows a significant decrease in gross cardiac function relative to controls. **A**, No difference between the EF of control (black circles) and iMgat1KO (blue triangles) mice was observed through 21 DPI. A sharp reduction in iMgat1KO EF occurred at 28 DPI relative to controls (58.0±3.2% vs 47.0±2.4%). The iMgat1KO EF continued to decrease through 168 DPI with no change in the control EF (168 DPI; 58.4±1.7% vs 33.4±2.2%) (global TCre effect P=0.002; interaction of TCre and DPI P<0.001). **B**, The FS followed the same trend (global TCre effect P=0.003; interaction of TCre and DPI P<0.001). Note that the *x* axes are nonlinear and *y* axes range from 24% to 75% in **A** and 10% to 45% in **B**. N=6/5 animals. Only significance between the groups at the same time point is indicated. Two-way repeated measures ANOVA and Sidak post hoc test. DPI indicates days post induction; EF, ejection fraction; FS, fractional shortening; iMgat1KO, tamoxifen-inducible, cardiomyocyte *Mgat1* knockout; KO, knockout; and TCre, tamoxifen-inducible Cre recombinase.

The Reduction in LV Systolic Function Is Not Associated With Cardiomyocyte Action Potential or Cardiomyocyte Potassium Current Remodeling

The cardiomyocyte AP is characterized by a rapid depolarization driven by the influx of Na^+ followed by a slower repolarization phase where inward Ca^{2+} currents are overcome by an efflux of K^+ through K_V.[14] HF in humans and animal models with cardiac insufficiency often presents with AP prolongation precipitated by a decreased efflux of I_K from cardiomyocytes.[58–60] We previously demonstrated this AP prolongation concomitant with reduced I_K that develops by ~8 to 16 weeks after embryonic ablation of GlcNAcT1 in the cMgat1KO model.[34,41] For reasons discussed previously, the cMgat1KO model could not be used to determine whether such cellular remodeling preceded or resulted from the onset of reduced systolic function in that model system. Thus, to determine if the gross contractile dysfunction in the iMgat1KO mice correlated with similar electrical remodeling at the cellular

level, and whether such remodeling preceded HFrEF onset, APs (Figure 5A) and K^+ currents (Figure 6A) were recorded from isolated cardiomyocytes before (11 to 14 DPI; early) and after (90 to 130 DPI; late) the onset of the reduced LVEF (starting at 28 DPI). Isolated cardiomyocyte AP recordings demonstrated no difference in resting membrane potentials or in AP amplitude or duration between control and iMgat1KO cardiomyocytes at either early or late time points (Figure 5).Net I_K traces from isolated cardiomyocytes were fit to a triexponential function to account for the contributing characteristics of the fast inactivating, transient currents; slow, rectifier-type currents, $I_{k,slow1}$ and $I_{K,slow2}$; and the constant, steady-state current, as done by our group previously.[34] Neither the peak outward current density (I_K) nor the amplitude of the contributing currents differed from control cardiomyocyte I_K before or after the reduced EF (Figure 6B). Following the onset of HFrEF, there was very little remodeling of I_K. Data demonstrated a significantly shorter time constant of transient currents (τ_{to}) (89±6.0 ms versus 71±4.7 ms) at the late time point (90–130 DPI; Figure 6C). Additionally, as shown previously,[34] a longer time constant was observed for $I_{K,slow2}$ without a change in amplitude in the iMgat1KO cardiomyocytes at the late time point ($\tau_{k,slow2}$) (5300±400 ms versus 6400±300 ms) (Figure 6C). These findings at the late timepoint might suggest the beginning stages of ion channel remodeling in iMgat1KO cardiomyocytes starting around 93 DPI. However, it should be noted that these subtle changes in I_K characteristics were observed 65 days after the observed reductions in EF (Figure 4A) and did not lead to observable AP prolongation (Figure 5).

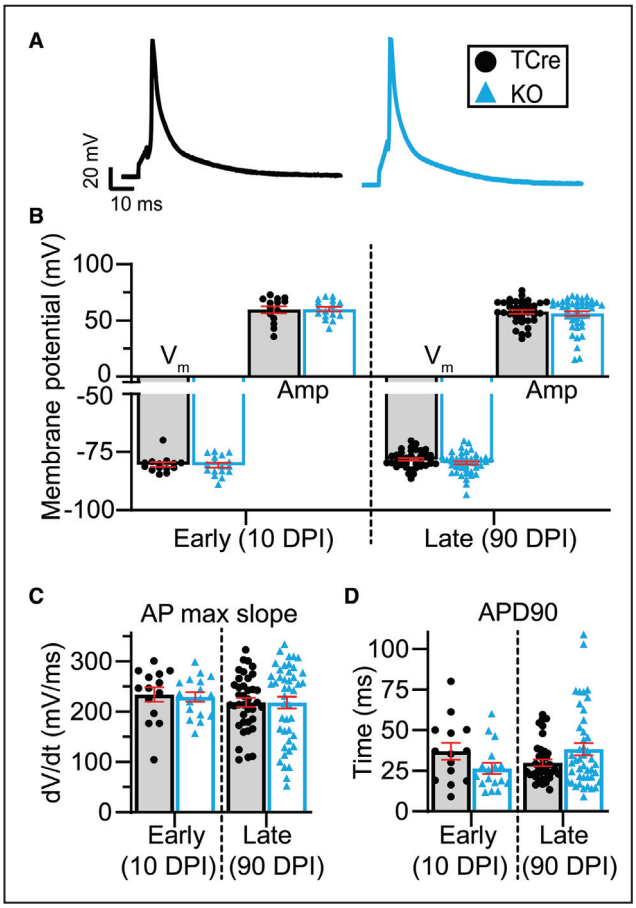

Figure 5. Ventricular action potentials in iMgat1KO cardiomyocytes.
APs measured in ventricular myocytes did not differ in the iMgat1KO mice compared with the controls at early (10–21 DPI) or late (90–130 DPI) time points. **A**, Representative whole cell APs from control (TCre; left, black) and iMgat1KO (right, blue) myocytes. **B**, Vm and amplitude were the same in the controls and iMgat1KO cardiomyocytes at both time points. (Control/iMgat1KO; early, Vm: −80.4±0.9 mV vs −80.7±1.0 mV; amplitude 59.5±3.0 mV vs 59.9±2.0 mV; late, Vm, rest: −78.4±0.6 mV vs −79.6±0.7 mV; amplitude 57.6±1.6 mV vs 56.1±2.1 mV. Unpaired, 2-tailed Student's *t* test). **C** and **D**, Similarly, no differences were observed in the maximum slope of depolarization or the duration to repolarization back to APD90 (early, max slope: 233.7±14.3 mV/ms vs 229.1±9.6 mV/ms; APD90: 37.0±5.2 ms vs 59.9±2.0 ms; late, max slope: 218.1±9.0 mV/ms vs 217.7±11.7 mV/ms; APD90 28.0±2.1 ms vs 38.3±3.6 ms. Mann–Whitney test). Early: N=2, n=14/17; late: N=5/6, n=38/44. AP indicates action potential; APD90, 90% of the peak voltage; DPI, days post induction; iMgat1KO, tamoxifen-inducible, cardiomyocyte *Mgat1* knockout; KO, knockout; TCre, tamoxifen-inducible Cre recombinase; and Vm, resting membrane potential.

Neither Cardiomyocyte Ca^{2+}-Handling Nor Contractility Dynamics Are Altered With the Induced Deletion of *Mgat1*, Acutely or Chronically

Cardiomyocyte contraction is dependent on voltage-sensitive Ca^{2+} currents initiating the release of Ca^{2+} stores into the cytoplasm to drive actin-myosin shortening. HFrEF has been shown to be associated with dyssynchronous Ca^{2+}-handling and diminished cardiomyocyte contractility, which contributes to the gross reduction in EF.[4,7] To assess if the gross cardiac dysfunction described herein is driven, even in part, by an accumulation of abnormal cardiomyocyte Ca^{2+} handling and EC coupling, intracellular Ca^{2+} transients (Figure 7A) and individual cardiomyocyte contractility (Figure 7D) were measured under field stimulation as described in the methods section and as done by us previously.[33,38] No differences were observed between iMgat1KO and control cardiomyocytes before (13–21 DPI) or after (90–130 DPI) the reduction in EF (starting at 28 DPI). The influx of Ca^{2+}, described by the amplitude (Figure 7B) and maximum slope of rise (Figure 7C) of the Ca^{2+} transients, was not different between the groups. These observations were consistent with that observed for cardiomyocyte contractility, as there was no change in the sarcomere FS (Figure 7F), maximum rate of contraction, or with relaxation (Figure 7G). Cardiomyocyte relaxation is reliant

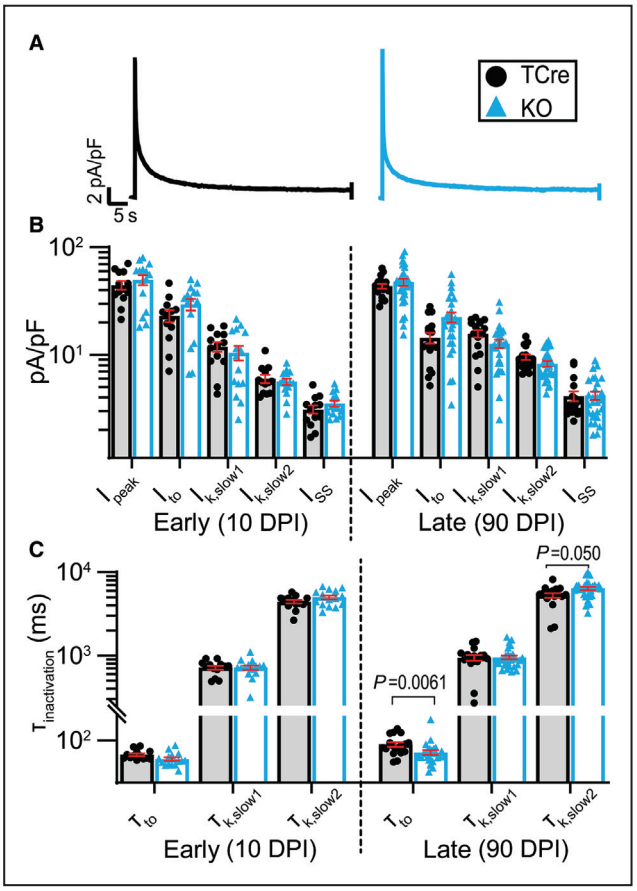

Figure 6. Cardiomyocyte, voltage-sensitive potassium currents.
Repolarizing (I_K) density remodeling did not precede the onset of HFrEF (early, 10–21 DPI), and only modest changes in contributing currents were observed afterward (late, 90–130 DPI). **A**, Representative whole cell I_K traces from a control (TCre; left, black) and iMgat1KO (right, blue) myocyte at the early time point. **B**, The amplitudes of the contributing I_K did not differ between the groups at the early (10 DPI) or late (90 DPI) time points for any of the I_K (unpaired, 2-tailed Student's *t* test corrected for 5 tests). **C**, The associated I_K inactivation rates did not differ at the early (10 DPI) time point. There was an observed decrease in the late (90 DPI) I_{to} inactivation rate (τ_{to}) and an increase in the late (90 DPI) $I_{K,slow\,2}$ inactivation rate ($\tau_{k,slow2}$; Mann–Whitney rank sum test corrected for 3 tests). Note that the *y* axes in (**B**) and (**C**) are logarithmic. Early: N=2, n=13/15; late: N=2, n=17/28. DPI indicates days post induction; HFrEF, heart failure with reduced ejection fraction; I_K, potassium current; iMgat1KO, tamoxifen-inducible, cardiomyocyte *Mgat1* knockout; KO, knockout; and TCre, tamoxifen-inducible Cre recombinase.

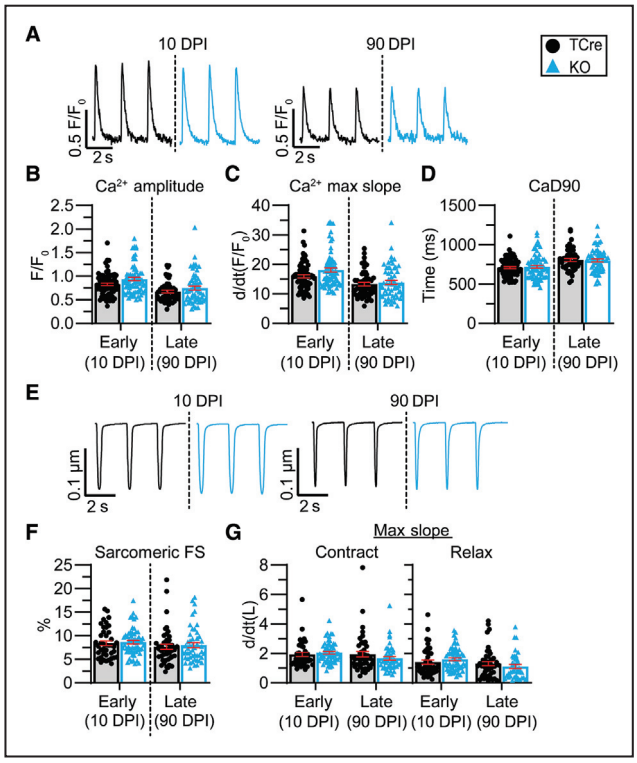

Figure 7. Cardiomyocyte calcium transients and contractility.
GlcNAcT1 deletion in the adult iMgat1KO mice did not disrupt intracellular Ca^{2+} transients or myocyte contractility. **A**, Example traces of intracellular Ca^{2+}–sensitive, ratiometric fluorescence of control (black) and iMgat1KO myocytes (blue) at the early (10–21 DPI) and late (90–130 DPI) time points. **B** through **D**, No changes in the amplitude, maximum slope of rise, or CaD90 were observed in the iMgat1KO cardiomyocytes. Early: N=4, n=76/73; late: N=5, n=52/58 (amplitude and max slope, unpaired, 2-tailed Student's *t* test; CaD90, Mann–Whitney rank-sum test). **E**, Representative sarcomere shortening traces of control (black) and iMgat1KO myocytes (blue) at early (10–21 DPI) and late (90–130 DPI) time points. **F** and **G**, The FS and the maximum rate of contraction and relaxation of the sarcomeres were not affected in the iMgat1KO cardiomyocytes relative the control cells. Early: N=2/3, n=41/59; late: N=5, n=46/49. Mann–Whitney rank sum test. CaD90 indicates duration to return to 90% of the peak; DPI, days post induction; FS, fractional shortening; GlcNAcT1, N-acetylglucosaminyltransferase I; iMgat1KO, tamoxifen-inducible, cardiomyocyte *Mgat1* knockout; KO, knockout; and TCre, tamoxifen-inducible Cre recombinase.

on the extrusion of Ca^{2+} from the cytoplasm back out of the cell or into intracellular stores. This process was also unaffected in the iMgat1KO model (Figure 7D and 7G). Each Ca^{2+} transient and contraction were consistent and did not vary beat to beat. These findings indicate that the direct effect of a rightward shift in Ca_v gating with *Mgat1* deletion is not sufficient to affect cardiomyocyte Ca^{2+} handling and contractility significantly. These data also suggest that the gross systolic dysfunction that presents as HFrEF is not likely caused entirely by electromechanical dysfunction of the individual cardiomyocyte.

DISCUSSION

Here, we demonstrate that deletion of GlcNAcT1 (encoded by *Mgat1*) in the adult mouse cardiomyocyte was sufficient to cause a significant reduction in LV systolic function by 4 weeks post-*Mgat1* deletion that continued regressing into HFrEF by around 8 weeks post induction (Figures 1 and 4; Table S1). This significant decline

in systolic function was nearly identical to that observed in the embryonic, cardiomyocyte-specific deletion of *Mgat1* model (cMgat1KO) previously characterized.[33,34] Also consistent with the cMgat1KO studies, the voltage-dependent gating of the direct GlcNAcT1 target, cardiomyocyte Ca_v, was shown to be significantly shifted to more depolarized potentials (Figure 3).[33] The data also indicate that adult deletion of the cardiomyocyte *Mgat1* leads to a similar reduction of complex/hybrid N-glycosylation in cardiomyocytes (Figure 1).

Although there was a consistent impact on LV contractility with the embryonic and adult deletion of *Mgat1*, the cardiomyocyte remodeling, ventricular dilation, and increased fibrosis that were observed in the diseased cMgat1KO were not observed in 28 through 90–130 DPI diseased iMgat1KO adult cardiomyocytes (if ever). That is, the progressive reduction in I_K that likely can contribute to the observed prolongation of the cardiomyocyte AP, as well as modest effects on cellular Ca^{2+} handling and sarcomere FS and the onset of significantly increased fibrosis that were reported for the cMgat1KO,[33,34,41] were not observed in the iMgat1KO at times post induction well beyond progression into HFrEF (Figures 2, 5 through 7). Further, only very modest changes in I_K, which do not likely contribute to significant ionic remodeling, were observed at any tested time point post induction. These data indicate that the cellular remodeling[10,61] and fibrosis[15] that can be observed in animal and human HF models[8] are not necessary to directly cause the reduced EF that is diagnostic for HFrEF in this model, but rather, are likely a result of disease progression, perhaps as compensatory (or decompensatory) mechanisms yet to be determined.

The postdevelopment deletion of *Mgat1* leads to a rapid and significant reduction in cardiac systolic function by 28 DPI that progresses further into HFrEF on or around 56 DPI (Figure 4). The longitudinal, echocardiographic study completed here illustrates the critical role of N-glycosylation in myocardial function, specifically including the need for cardiomyocyte hybrid/complex N-glycosylation (even post development) in maintaining the integrity of cardiac electromechanical function(s). This decrease in systolic function did not coincide with a similar structural LV wall thinning characteristic of DCM development following other models of disrupted glycosylation[33,36]; rather, there was a slight thickening of the LV anterior wall in the iMgat1KO after the onset of HFrEF (Tables S1, S2).[33]

HFrEF can lead to cardiomyocyte remodeling due to the complex neurohormonal control of the heart.[3,9,10,62] Distinguishing initial causes of HF from disease-related (compensatory or decompensatory) changes to cardiomyocyte physiology is a difficult challenge. However, the longitudinal echocardiographic study completed here provides a distinct timeline for when cardiac contractility becomes impaired and thus allows one to determine whether cellular remodeling events precede, and possibly initiate, systolic dysfunction from compensatory or decompensatory changes in cardiomyocyte activity that follow the onset of HF.

It is generally accepted that direct insults at the cardiomyocyte level, such as disruption of t-tubules,[6,63,64] calcium-handling, and EC coupling,[65,66] can contribute to an aggregation of cardiac dysfunction and HFrEF.[61,62,67] Here, cellular electromechanical studies were completed on isolated cardiomyocytes before and after the onset of gross dysfunction to assess the functional cardiomyocyte health and to determine if cellular remodeling contributed to the observed cardiac dysfunction (Figures 5 through 7). Current dogma suggests that remodeling includes a resulting prolongation of the cardiomyocyte AP that is driven via a reduction in potassium currents with HF.[8,12,14] The iMgat1KO cardiomyocytes did not display any changes in ventricular AP waveform relative to controls before or even 60 days after the onset of HFrEF (Figure 5). Consistently, there was little to no I_K remodeling relative to the control cardiomyocytes at the examined time points (Figure 6).

Intracellular Ca^{2+} transients and contractility can be affected in HFrEF. Slow intracellular calcium transients with reduced amplitudes are associated with chronic HF and contribute to reduced cardiomyocyte contractility,[62,65,68] though Mork et al showed a transitory increase in the amplitudes of sarcomeric shortening and intracellular calcium transients early after an ischemic injury that progressed to diminished function later.[69] Here, intracellular Ca^{2+} transients and contractility dynamics of the isolated iMgat1KO cardiomyocytes did not indicate abnormal function at ~10 or at ~90 DPI (Figure 7). Thus, despite there being significantly reduced LV contractility beginning at 28 DPI, there was no significant or measurable impact on cardiomyocyte contractility that preceded or followed the onset of the gross LV dysfunction. This lack of dysfunction on the individual myocytes could suggest that either the observed small shifts in Ca_v gating in the iMgat1KO cardiomyocytes are responsible for the reduced systolic function (without changing AP waveform or cytosolic Ca^{2+} dynamics), or reduced N-glycosylation could be affecting the cardiomyocyte-to-cardiomyocyte electromechanical coupling such that LV contractility is reduced.

To that end, cardiac fibrosis is a common contributor to decreased cardiac hemodynamics in HF and could explain increased cardiac dysfunction of the whole heart.[57] Cardiac fibrosis can be a result of fibrotic replacement after cardiomyocyte death or a result of fibroblast activation following increased cardiac pressure and stress, which both result in increased collagen deposition in the extracellular matrix.[57,70,71] Although increased fibrosis would likely contribute to

aberrant tissue-level electromechanical activity, we observed that there was no increase in cardiac collagen deposition before or following HFrEF onset (at 10, 47, and 132 DPI; Figure 2B). This suggests that increased fibrosis does not contribute to HFrEF onset in this model and thus is not a likely mechanism by which intercellular electromechanical activity is impaired with reduced complex/hybrid N-glycosylation.

Proper cardiac activity is dependent on cardiomyocyte (eg, APs and contractility) and tissue-level (eg, cardiomyocyte-to-cardiomyocyte signaling) electromechanical activity.[15,72] We demonstrate here that the reduced hybrid/complex N-glycosylation in our iMgat1KO model does not have a significant impact on the AP, calcium handling, or contractility of isolated cardiomyocytes (Figures 5 through 7). This could suggest that the significantly reduced LV EF shown here may be secondary to disruption of the electromechanical coupling between cardiomyocytes. Briefly, cardiomyocytes are longitudinally linked at the dense ICD structures. Within the ICDs, junctions composed of desmosomes and adherens junctions mechanically anchor one cell to the next, and gap junctions, made of connexons, electrically couple adjacent cardiomyocytes.[73] Members of the cadherin superfamily of transmembrane proteins are responsible for the extracellular bonds across these mechanical junctions, including N-cadherin,[74] desmoglein-2,[75] and desmocollin-2,[76] all 3 of which have been shown to contain N-glycosylation sites that may be direct targets of GlcNAcT1. Therefore, it is important for future studies to determine if the disrupted N-glycosylation in our iMgat1KO hearts is affecting these necessary structures. The connexin proteins, primarily connexin-43, responsible for making up the gap junctions, do not contain an N-glycosylation site and would not be directly affected in our model. However, it has been shown that the successful formation or distribution of cardiomyocyte gap junctions is dependent on the normal function of the mechanical cadherins within the ICD.[77,78] Therefore, in addition to the direct disruption of adherens junctions and desmosomes in this model, an indirect effect on the coupling of gap junctions may also be possible.

Na_V are also clustered within microdomains extending from the gap junctions in cardiomyocyte ICDs.[79] Studies have shown that N-linked sialic acid on the Na_V α-, β_1-, and β_2 subunits directly modulate Na_V gating[28,80] and was confirmed within our cMgat1KO model.[34] It is thought that Na_V channels clustered around the gap junctions contribute to intercellular ephaptic conduction. This mechanism is facilitated by the ICD-localized I_{Na} of the prejunctional cardiomyocyte, which removes extracellular positive charge from the junctional space. This results in the effective depolarization of the postjunctional membrane, thereby promoting postjunctional Na_V activity and enhancing cell-to-cell conduction.[81] Modeling and experimental evidence has shown that this conduction is dependent on the number of Na_V near the gap junctions as well as the geometry/size of the cleft between the adjacent cells.[82–84]

Thus, if prejunctional Na_V activity promotes postjunctional Na_V activity as proposed above, then the direct effects of reduced N-glycosylation (and thereby sialic acids) on ICD-localized Na_V, could be responsible for reduced Na_V activity of pre- and postjunctional Na_V through well-established electrostatic mechanisms,[28,34] thereby effectively slowing cell-to-cell conduction. It is also quite possible that bulk structural effects of the Na_V (and other ICD protein) N-glycans effectively alter the cleft geometry and thereby ephaptic conduction or mechanical signaling between myocytes. Certainly, both potential mechanisms are feasible and will be the focus of future studies. As just 1 example, reduced N-glycosylation could modulate interactions between Na_V α and β subunits within and between neighboring cardiomyocytes, potentially altering α-subunit voltage-dependent gating through electrostatic mechanisms as well as β-subunit adhesion properties within and across the junctions.[85] The iMgat1KO model described here offers a robust experimental model that can be used to address these questions.

This work expands on previous studies that examined the role of N-glycosylation on VGICs and cardiomyocytes in cellular and animal models under various means of altering N-glycosylation through pharmacologic inhibition and transgenic manipulation.[28,30,36,80] As referenced in the introduction, aberrant glycosylation has been associated with a variety of clinical diseases that negatively affect cardiac function, including HF secondary to congenital disorders of glycosylation,[23] idiopathic DCM,[27] and Brugada syndrome.[37] The iMgat1KO mouse model also provides a tool to explore the feasibility of potential therapeutic targets in future translational investigations.

CONCLUSIONS

In summary, here we demonstrate that a reduction in hybrid/complex N-glycosylation in the adult mouse modulates Ca_V gating that is, however, not sufficient to induce significant cardiomyocyte electromechanical remodeling before the onset of HFrEF (if ever). The data also show that, by 4 weeks post-*Mgat1* deletion, there is a significant reduction in LV contractility (EF/FS) that progresses into HFrEF by around 8 weeks post induction but in the absence of any cardiomyocyte remodeling and without an increase in fibrosis. Thus, in addition to allowing one to determine mechanisms by which reduced N-glycosylation can cause adult-onset

HFrEF, this novel model is well suited to investigate the tissue-level mechanisms responsible for inducing reduced systolic function that progresses into HFrEF in the absence of (or at least before) cardiomyocyte remodeling and fibrosis. Although there is an acute effect of complex N-glycans on Ca_V gating, this alone, as described, is very unlikely to be able to explain fully the LV-level reduction in electromechanical activity. It is possible that earlier (pre- and perinatal) changes in hybrid/complex N-glycosylation could have additional effects on cardiomyocyte and cardiac electromechanical activities—data indicate that N-glycans do vary in the heart over time.[29,86] Thus, a thorough comparison of the previously described cMgat1KO[33,34] with the iMgat1KO model outlined here could be useful in defining such development-dependent effects. Regardless of potential developmental effects, the data here indicate that there is also an effect of complex N-glycosylation on tissue-level electromechanical activities in the adult (in the absence of increased fibrosis) that cannot be explained fully by changes in electromechanical activities of the individual cardiomyocyte.

ARTICLE INFORMATION

Received May 16, 2024; accepted September 17, 2024.

Affiliation

Department of Neuroscience, Cell Biology & Physiology, Boonshoft School of Medicine and College of Science and Mathematics, Wright State University, Dayton, OH.

Acknowledgments

We would like to thank Dr Ramzi Nahhas from the Boonshoft School of Medicine at Wright State University for his expert assistance with RStudio for the statistical analysis of the cellular and fibrosis data.

Sources of Funding

This work was supported by the National Science Foundation, Division of Molecular and Cellular Biosciences grant – 1856199 (to ESB and ARE).

Disclosures

None.

Supplemental Material

Data S1

REFERENCES

1. Savarese G, Becher PM, Lund LH, Seferovic P, Rosano GMC, Coats AJS. Global burden of heart failure: a comprehensive and updated review of epidemiology. *Cardiovasc Res*. 2023;118:3272–3287. doi: 10.1093/cvr/cvac013
2. Heidenreich PA, Bozkurt B, Aguilar D, Allen LA, Byun JJ, Colvin MM, Deswal A, Drazner MH, Dunlay SM, Evers LR, et al. AHA/ACC/HFSA guideline for the management of heart failure: a report of the American College of Cardiology/American Heart Association joint committee on clinical practice guidelines. *Circulation*. 2022;2022:145. doi: 10.1161/cir.0000000000001063
3. Kilfoil PJ, Lotteau S, Zhang R, Yue X, Aynaszyan S, Solymani RE, Cingolani E, Marbán E, Goldhaber JI. Distinct features of calcium handling and β-adrenergic sensitivity in heart failure with preserved versus reduced ejection fraction. *J Physiol*. 2020;598:5091–5108. doi: 10.1113/jp280425
4. Frisk M, Ruud M, Espe EKS, Aronsen JM, Røe ÅT, Zhang L, Norseng PA, Sejersted OM, Christensen GA, Sjaastad I, et al. Elevated ventricular wall stress disrupts cardiomyocyte t-tubule structure and calcium homeostasis. *Cardiovasc Res*. 2016;112:443–451. doi: 10.1093/cvr/cvw111
5. Louch WE. A horse of a different colour: distinct mechanisms of HFpEF and HFrEF. *J Physiol*. 2020;598:5005–5006. doi: 10.1113/jp280691
6. Louch WE, Mørk HK, Sexton J, Strømme TA, Laake P, Sjaastad I, Sejersted OM. T-tubule disorganization and reduced synchrony of Ca2+ release in murine cardiomyocytes following myocardial infarction. *J Physiol*. 2006;574:519–533. doi: 10.1113/jphysiol.2006.107227
7. Zima AV, Bovo E, Mazurek SR, Rochira JA, Li W, Terentyev D. Ca handling during excitation–contraction coupling in heart failure. *Pflugers Arch Eur J Physiol*. 2014;466:1129–1137. doi: 10.1007/s00424-014-1469-3
8. Beuckelmann DJ, Näbauer M, Erdmann E. Alterations of K+ currents in isolated human ventricular myocytes from patients with terminal heart failure. *Circ Res*. 1993;73:379–385. doi: 10.1161/01.res.73.2.379
9. Husti Z, Varró A, Baczkó I. Arrhythmogenic remodeling in the failing heart. *Cells*. 2021;10:3203. doi: 10.3390/cells10113203
10. Janse MJ. Electrophysiological changes in heart failure and their relationship to arrhythmogenesis. *Cardiovasc Res*. 2004;61:208–217. doi: 10.1016/j.cardiores.2003.11.018
11. Long VP, Bonilla IM, Vargas-Pinto P, Nishijima Y, Sridhar A, Li C, Mowrey K, Wright P, Velayutham M, Kumar S, et al. Heart failure duration progressively modulates the arrhythmia substrate through structural and electrical remodeling. *Life Sci*. 2015;123:61–71. doi: 10.1016/j.lfs.2014.12.024
12. Näbauer M. Potassium channel down-regulation in heart failure. *Cardiovasc Res*. 1998;37:324–334. doi: 10.1016/s0008-6363(97)00274-5
13. Sah R, Ramirez RJ, Oudit GY, Gidrewicz D, Trivieri MG, Zobel C, Backx PH. Regulation of cardiac excitation–contraction coupling by action potential repolarization: role of the transient outward potassium current Ito. *J Physiol*. 2003;546:5–18. doi: 10.1113/jphysiol.2002.026468
14. Yang K-C, Nerbonne JM. Mechanisms contributing to myocardial potassium channel diversity, regulation and remodeling. *Trends Cardiovasc Med*. 2016;26:209–218. doi: 10.1016/j.tcm.2015.07.002
15. King JH, Huang CL-H, Fraser JA. Determinants of myocardial conduction velocity: implications for arrhythmogenesis. *Front Physiol*. 2013;4:154. doi: 10.3389/fphys.2013.00154
16. Bieberich E. Synthesis, processing, and function of N-glycans in N-glycoproteins. *Adv Neurobiol*. 2014;9:47–70. doi: 10.1007/978-1-4939-1154-7_3
17. Varki A. Biological roles of glycans. *Glycobiology*. 2017;27:3–49. doi: 10.1093/glycob/cww086
18. Lau KS, Partridge EA, Grigorian A, Silvescu CI, Reinhold VN, Demetriou M, Dennis JW. Complex N-glycan number and degree of branching cooperate to regulate cell proliferation and differentiation. *Cell*. 2007;129:123–134. doi: 10.1016/j.cell.2007.01.049
19. Schachter H. The joys of HexNAc. The synthesis and function of N- and O-glycan branches. *Glycoconj J*. 2000;17:465–483. doi: 10.1023/a:1011010206774
20. Stanley P. What have we learned from glycosyltransferase knockouts in mice? *J Mol Biol*. 2016;428:3166–3182. doi: 10.1016/j.jmb.2016.03.025
21. Chang IJ, He M, Lam CT. Congenital disorders of glycosylation. *Ann Transl Med*. 2018;6:477. doi: 10.21037/atm.2018.10.45
22. Gehrmann J, Sohlbach K, Linnebank M, Böhles HJ, Buderus S, Kehl HG, Vogt J, Harms E, Marquardt T. Cardiomyopathy in congenital disorders of glycosylation. *Cardiol Young*. 2003;13:345–351. doi: 10.1017/S1047951103000702
23. Marques-Da-Silva D, Francisco R, Webster D, Dos Reis FV, Jaeken J, Pulinilkunnil T. Cardiac complications of congenital disorders of glycosylation (CDG): a systematic review of the literature. *J Inherit Metab Dis*. 2017;40:657–672. doi: 10.1007/s10545-017-0066-y
24. Yang WS, Grover S, Smith E, Selvanayagam JB. A rare case report of type 1 congenital disorders of glycosylation with acute decompensated heart failure and the incidental discovery of congenital disorders of glycosylation associated dilated cardiomyopathy and acute myocarditis. *Eur Heart J Case Rep*. 2024;8:ytae088. doi: 10.1093/ehjcr/ytae088
25. Barrans JD, Allen PD, Stamatiou D, Dzau VJ, Liew CC. Global gene expression profiling of end-stage dilated cardiomyopathy using a human cardiovascular-based cDNA microarray. *Am J Pathol*. 2002;160:2035–2043. doi: 10.1016/S0002-9440(10)61153-4

26. Hwang JJ, Allen PD, Tseng GC, Lam CW, Fananapazir L, Dzau VJ, Liew CC. Microarray gene expression profiles in dilated and hypertrophic cardiomyopathic end-stage heart failure. *Physiol Genomics*. 2002;10:31–44. doi: 10.1152/physiolgenomics.00122.2001
27. Yung CK, Halperin VL, Tomaselli GF, Winslow RL. Gene expression profiles in end-stage human idiopathic dilated cardiomyopathy: altered expression of apoptotic and cytoskeletal genes. *Genomics*. 2004;83:281–297. doi: 10.1016/j.ygeno.2003.08.007
28. Stocker PJ, Bennett ES. Differential sialylation modulates voltage-gated Na+ channel gating throughout the developing myocardium. *J Gen Physiol*. 2006;127:253–265. doi: 10.1085/jgp.200509423
29. Montpetit ML, Stocker PJ, Schwetz TA, Harper JM, Norring SA, Schaffer L, North SJ, Jang-Lee J, Gilmartin T, Head SR, et al. Regulated and aberrant glycosylation modulate cardiac electrical signaling. *Proc Natl Acad Sci*. 2009;106:16517–16522. doi: 10.1073/pnas.0905414106
30. Ednie AR, Bennett ES. Modulation of voltage-gated ion channels by sialylation. *Compr Physiol*. 2012;2:1269–1301. doi: 10.1002/cphy.c110044
31. Ednie AR, Harper JM, Bennett ES. Sialic acids attached to N- and O-glycans within the Nav1.4 D1S5-S6 linker contribute to channel gating. *Biochim Biophys Acta*. 2015;1850:307–317. doi: 10.1016/j.bbagen.2014.10.027
32. Ednie AR, Horton KK, Wu J, Bennett ES. Expression of the sialyltransferase, ST3Gal4, impacts cardiac voltage-gated sodium channel activity, refractory period and ventricular conduction. *J Mol Cell Cardiol*. 2013;59:117–127. doi: 10.1016/j.yjmcc.2013.02.013
33. Ednie AR, Deng W, Yip KP, Bennett ES. Reduced myocyte complex N-glycosylation causes dilated cardiomyopathy. *FASEB J*. 2019;33:1248–1261. doi: 10.1096/fj.201801057R
34. Ednie AR, Parrish AR, Sonner MJ, Bennett ES. Reduced hybrid/complex N-glycosylation disrupts cardiac electrical signaling and calcium handling in a model of dilated cardiomyopathy. *J Mol Cell Cardiol*. 2019;132:13–23. doi: 10.1016/j.yjmcc.2019.05.001
35. Ednie AR, Bennett ES. Reduced sialylation impacts ventricular repolarization by modulating specific K+ channel isoforms distinctly. *J Biol Chem*. 2015;290:2769–2783. doi: 10.1074/jbc.m114.605139
36. Deng W, Ednie AR, Qi J, Bennett ES. Aberrant sialylation causes dilated cardiomyopathy and stress-induced heart failure. *Basic Res Cardiol*. 2016;111:57. doi: 10.1007/s00395-016-0574-1
37. Ghiroldi A, Ciconte G, Creo P, Tarantino A, Melgari D, D'Imperio S, Piccoli M, Cirillo F, Micaglio E, Monasky MM, et al. Alterations of the sialylation machinery in Brugada syndrome. *Int J Mol Sci*. 2022;23:13154. doi: 10.3390/ijms232113154
38. Ednie AR, Bennett ES. Intracellular O-linked glycosylation directly regulates cardiomyocyte L-type Ca(2+) channel activity and excitation-contraction coupling. *Basic Res Cardiol*. 2020;115:59. doi: 10.1007/s00395-020-00820-0
39. Ednie AR, Paul-Onyia CD, Bennett ES. Reduced O-GlcNAcylation diminishes cardiomyocyte Ca(2+) dependent facilitation and frequency dependent acceleration of relaxation. *J Mol Cell Cardiol*. 2023;180:10–21. doi: 10.1016/j.yjmcc.2023.04.007
40. Schwarz F, Aebi M. Mechanisms and principles of N-linked protein glycosylation. *Curr Opin Struct Biol*. 2011;21:576–582. doi: 10.1016/j.sbi.2011.08.005
41. Kim H, Yang H, Ednie AR, Bennett ES. Simulation modeling of reduced glycosylation effects on potassium channels of mouse Cardiomyocytes. *Front Physiol*. 2022;13:816651. doi: 10.3389/fphys.2022.816651
42. Wang L, Feng Z-P, Kondo CS, Sheldon RS, Duff HJ. Developmental changes in the delayed rectifier K^+ channels in mouse heart. *Circ Res*. 1996;79:79–85. doi: 10.1161/01.res.79.1.79
43. Franzka P, Krüger L, Schurig MK, Olecka M, Hoffmann S, Blanchard V, Hübner CA. Altered glycosylation in the aging heart. *Front Mol Biosci*. 2021;8:8. doi: 10.3389/fmolb.2021.673044
44. Percie du Sert NHV, Ahluwalia A, Alam S, Avey MT, Baker M, Browne WJ, Clark A, Cuthill IC, Dirnagl U, Emerson M, et al. The ARRIVE Guidelines 2.0: updated guidelines for reporting animal research. 2020.
45. Ye Z. N-glycan branching requirement in neuronal and postnatal viability. *Glycobiology*. 2004;14:547–558. doi: 10.1093/glycob/cwh069
46. Bersell K, Choudhury S, Mollova M, Polizzotti BD, Ganapathy B, Walsh S, Wadugu B, Arab S, Kühn B. Moderate and high amounts of tamoxifen in α-MHC-MerCreMer mice induce a DNA damage response, leading to heart failure and death. *Dis Model Mech*. 2013;6:1459–1469. doi: 10.1242/dmm.010447
47. Andersson KB, Winer LH, Mørk HK, Molkentin JD, Jaisser F. Tamoxifen administration routes and dosage for inducible Cre-mediated gene disruption in mouse hearts. *Transgenic Res*. 2010;19:715–725. doi: 10.1007/s11248-009-9342-4
48. Fuller W, Eaton P, Bell JR, Shattock MJ. Ischemia-induced phosphorylation of phospholemman directly activates rat cardiac Na/K ATPase. *FASEB J*. 2004;18:197–199. doi: 10.1096/fj.03-0213fje
49. Van Damme EJM, Allen AK, Peumans WJ. Isolation and characterization of a lectin with exclusive specificity towards mannose from snowdrop (*Galanthus nivalis*) bulbs. *FEBS Lett*. 1987;215:140–144. doi: 10.1016/0014-5793(87)80129-1
50. Ness TL, Robinson RL, Mojadedi W, Peavy L, Weiland MH. A streamlined Western blot exercise: an efficient and greener approach in the laboratory classroom. *Biochem Mol Biol Educ*. 2015;43:358–365. doi: 10.1002/bmb.20876
51. Ladner CL, Yang J, Turner RJ, Edwards RA. Visible fluorescent detection of proteins in polyacrylamide gels without staining. *Anal Biochem*. 2004;326:13–20. doi: 10.1016/j.ab.2003.10.047
52. O'Connell TD, Rodrigo MC, Simpson PC. Isolation and culture of adult mouse cardiac myocytes. *Methods in Molecular Biology*. Humana Press; 2007:271–296.
53. Schindelin J, Arganda-Carreras I, Frise E, Kaynig V, Longair M, Pietzsch T, Preibisch S, Rueden C, Saalfeld S, Schmid B, et al. Fiji: an open-source platform for biological-image analysis. *Nat Methods*. 2012;9:676–682. doi: 10.1038/nmeth.2019
54. Ruifrok AC, Johnston DA. Quantification of histochemical staining by color deconvolution. *Anal Quant Cytol Histol*. 2001;23:291–299.
55. Wilcox PMaR. Robust statistical methods in R using the WRS2 package. *Behav Res Methods*. 2020;52:52–488. doi: 10.3758/s13428-019-01246-w
56. Boulaksil M, Bierhuizen MF, Engelen MA, Stein M, Kok BJ, van Amersfoorth SC, Vos MA, van Rijen HV, de Bakker JM, van Veen TA. Spatial heterogeneity of Cx43 is an arrhythmogenic substrate of polymorphic ventricular tachycardias during compensated cardiac hypertrophy in rats. *Front Cardiovasc Med*. 2016;3:5. doi: 10.3389/fcvm.2016.00005
57. Kong P, Christia P, Frangogiannis NG. The pathogenesis of cardiac fibrosis. *Cell Mol Life Sci*. 2014;71:549–574. doi: 10.1007/s00018-013-1349-6
58. Kääb S, Dixon J, Duc J, Ashen D, NäBauer M, Beuckelmann DJ, Steinbeck G, Mckinnon D, Tomaselli GF. Molecular basis of transient outward potassium current downregulation in human heart failure. *Circulation*. 1998;98:1383–1393. doi: 10.1161/01.cir.98.14.1383
59. Kääb S, Nuss HB, Chiamvimonvat N, O'Rourke B, Pak PH, Kass DA, Marban E, Tomaselli GF. Ionic mechanism of action potential prolongation in ventricular myocytes from dogs with pacing-induced heart failure. *Circ Res*. 1996;78:262–273. doi: 10.1161/01.res.78.2.262
60. Cutler MJ, Rosenbaum DS, Dunlap ME. Structural and electrical remodeling as therapeutic targets in heart failure. *J Electrocardiol*. 2007;40:S1–S7. doi: 10.1016/j.jelectrocard.2007.05.027
61. Shou J, Huo Y. Changes of calcium cycling in HFrEF and HFpEF. *Mechanobiol Med*. 2023;1:100001–100005. doi: 10.1016/j.mbm.2023.100001
62. Ge Z, Li A, Mcnamara J, Dos Remedios C, Lal S. Pathogenesis and pathophysiology of heart failure with reduced ejection fraction: translation to human studies. *Heart Fail Rev*. 2019;24:743–758. doi: 10.1007/s10741-019-09806-0
63. Chen BY, Li Y, Jiang SX, Xie YP, Guo A, Kutschke W, Zimmerman K, Weiss RM, Miller FJ, Anderson ME, et al. β-Adrenergic receptor antagonists ameliorate myocyte T-tubule remodeling following myocardial infarction. *FASEB J*. 2012;26:2531–2537. doi: 10.1096/fj.11-199505
64. Wang S, Zhou Y, Luo Y, Kan R, Chen J, Xuan H, Wang C, Chen J, Xu T, Li D. SERCA2a ameliorates cardiomyocyte T-tubule remodeling via the calpain/JPH2 pathway to improve cardiac function in myocardial ischemia/reperfusion mice. *Sci Rep*. 2021;11:2037. doi: 10.1038/s41598-021-81570-4
65. Gwathmey JK, Copelas L, Mackinnon R, Schoen FJ, Feldman MD, Grossman W, Morgan JP. Abnormal intracellular calcium handling in myocardium from patients with end-stage heart failure. *Circ Res*. 1987;61:70–76. doi: 10.1161/01.res.61.1.70
66. Mercadier JJ, Lompré AM, Duc P, Boheler KR, Fraysse JB, Wisnewsky C, Allen PD, Komajda M, Schwartz K. Altered sarcoplasmic reticulum Ca2(+)-ATPase gene expression in the human ventricle during end-stage heart failure. *J Clin Invest*. 1990;85:305–309. doi: 10.1172/jci114429
67. Yano M, Ikeda Y, Matsuzaki M. Altered intracellular Ca^{2+} handling in heart failure. *J Clin Invest*. 2005;115:556–564. doi: 10.1172/jci24159

68. Benitah J-P, Perrier R, Mercadier J-J, Pereira L, Gómez AM. RyR2 and calcium release in heart failure. *Front Physiol*. 2021;12:734210. doi: 10.3389/fphys.2021.734210
69. Mork HK, Sjaastad I, Sande JB, Periasamy M, Sejersted OM, Louch WE. Increased cardiomyocyte function and Ca^{2+} transients in mice during early congestive heart failure. *J Mol Cell Cardiol*. 2007;43:177–186. doi: 10.1016/j.yjmcc.2007.05.004
70. Galati G, Leone O, Pasquale F, Olivotto I, Biagini E, Grigioni F, Pilato E, Lorenzini M, Corti B, Foà A, et al. Histological and histometric characterization of myocardial fibrosis in end-stage hypertrophic cardiomyopathy. *Circ Heart Fail*. 2016;9:e003090. doi: 10.1161/circheartfailure.116.003090
71. Liu J, Zhao S, Yu S, Wu G, Wang D, Liu L, Song J, Zhu Y, Kang L, Wang J, et al. Patterns of replacement fibrosis in hypertrophic cardiomyopathy. *Radiology*. 2022;302:298–306. doi: 10.1148/radiol.2021210914
72. Lei M, Salvage SC, Jackson AP, Huang CL. Cardiac arrhythmogenesis: roles of ion channels and their functional modification. *Front Physiol*. 2024;15:1342761. doi: 10.3389/fphys.2024.1342761
73. Vermij SH, Abriel H, van Veen TA. Refining the molecular organization of the cardiac intercalated disc. *Cardiovasc Res*. 2017;113:259–275. doi: 10.1093/cvr/cvw259
74. Guo H-B, Johnson H, Randolph M, Pierce M. Regulation of homotypic cell-cell adhesion by branched N-glycosylation of N-cadherin extracellular EC2 and EC3 domains. *J Biol Chem*. 2009;284:34986–34997. doi: 10.1074/jbc.m109.060806
75. Debus JD, Milting H, Brodehl A, Kassner A, Anselmetti D, Gummert J, Gaertner-Rommel A. In vitro analysis of arrhythmogenic cardiomyopathy associated desmoglein-2 (DSG2) mutations reveals diverse glycosylation patterns. *J Mol Cell Cardiol*. 2019;129:303–313. doi: 10.1016/j.yjmcc.2019.03.014
76. Brodehl A, Stanasiuk C, Anselmetti D, Gummert J, Milting H. Incorporation of desmocollin-2 into the plasma membrane requires N-glycosylation at multiple sites. *FEBS Open Bio*. 2019;9:996–1007. doi: 10.1002/2211-5463.12631
77. Li J, Levin MD, Xiong Y, Petrenko N, Patel VV, Radice GL. N-cadherin haploinsufficiency affects cardiac gap junctions and arrhythmic susceptibility. *J Mol Cell Cardiol*. 2008;44:597–606. doi: 10.1016/j.yjmcc.2007.11.013
78. Meyer RA, Laird DW, Revel JP, Johnson RG. Inhibition of gap junction and adherens junction assembly by connexin and A-CAM antibodies. *J Cell Biol*. 1992;119:179–189. doi: 10.1083/jcb.119.1.179
79. Agullo-Pascual E, Lin X, Leo-Macias A, Zhang M, Liang F-X, Li Z, Pfenniger A, Lübkemeier I, Keegan S, Fenyö D, et al. Super-resolution imaging reveals that loss of the C-terminus of connexin43 limits microtubule plus-end capture and NaV1.5 localization at the intercalated disc. *Cardiovasc Res*. 2014;104:371–381. doi: 10.1093/cvr/cvu195
80. Johnson D, Montpetit ML, Stocker PJ, Bennett ES. The sialic acid component of the β1 subunit modulates voltage-gated Sodium Channel function. *J Biol Chem*. 2004;279:44303–44310. doi: 10.1074/jbc.m408900200
81. Sperelakis N, Mann JE Jr. Evaluation of electric field changes in the cleft between excitable cells. *J Theor Biol*. 1977;64:71–96. doi: 10.1016/0022-5193(77)90114-x
82. Mori Y, Fishman GI, Peskin CS. Ephaptic conduction in a cardiac strand model with 3D electrodiffusion. *Proc Natl Acad Sci*. 2008;105:6463–6468. doi: 10.1073/pnas.0801089105
83. Veeraraghavan R, Lin J, Hoeker GS, Keener JP, Gourdie RG, Poelzing S. Sodium channels in the Cx43 gap junction perinexus may constitute a cardiac ephapse: an experimental and modeling study. *Pflugers Arch - Eur J Physiol*. 2015;467:2093–2105. doi: 10.1007/s00424-014-1675-z
84. Nowak MB, Veeraraghavan R, Poelzing S, Weinberg SH. Cellular size, gap junctions, and sodium channel properties govern developmental changes in cardiac conduction. *Front Physiol*. 2021;12:731025. doi: 10.3389/fphys.2021.731025
85. Veeraraghavan R, Hoeker GS, Alvarez-Laviada A, Hoagland D, Wan X, King DR, Sanchez-Alonso J, Chen C, Jourdan J, Isom LL, et al. The adhesion function of the sodium channel beta subunit (β1) contributes to cardiac action potential propagation. *elife*. 2018;7:37610. doi: 10.7554/eLife.37610
86. Contessotto P, Ellis BW, Jin C, Karlsson NG, Zorlutuna P, Kilcoyne M, Pandit A. Distinct glycosylation in membrane proteins within neonatal versus adult myocardial tissue. *Matrix Biol*. 2020;85–86:173–188. doi: 10.1016/j.matbio.2019.05.001

SUPPLEMENTAL MATERIAL

Table S1 Summary of echocardiographic parameters comparing TCre and iMgat1KO mice

Parameter		TCre			iMgat1KO	
Time	**Baseline**	**14 dpi**	**168 dpi**	**Baseline**	**14 dpi**	**168 dpi**
Rate (BPM)	408 ±17	401 ± 7	379 ± 7	381 ± 21	410 ± 7	370 ± 10
EF (%)	59.5 ± 2.4	60.3 ± 3.0	58.4 ± 1.7	59.7 ± 0.8	59.0 ± 1.2	33.4 ± 1.7$^{\#\#}$
FS (%)	31.5 ± 1.7	32.4 ± 2.0	30.6 ± 1.1	31.2 ± 0.5	31.1 ± 0.8	15.7 ± 0.9$^{\#\#}$
Diastole (mm)						
LVID	4.32 ± 0.14	4.64 ± 0.18	4.23 ± 0.15	3.91 ± 0.28	4.33 ± 0.11	3.53 ± 0.46
LVAW	0.90 ± 0.12	0.99 ± 0.09	0.81 ± 0.04	0.84 ± 0.05	0.93 ± 0.04	1.07 ± 0.06$^{\#}$
LVPW	0.90 ± 0.08	0.92 ± 0.07	0.95 ± 0.07	0.96 ± 0.08	0.86 ± 0.08	1.80 ± 0.43
Systole (mm)						
LVID	2.93 ± 0.12	3.12 ± 0.20	2.95 ± 0.13	2.58 ± 0.18	2.95 ± 0.10	3.04 ± 0.33$^{\#}$
LVAW	1.20 ± 0.14	1.51 ± 0.09	1.26 ± 0.06	1.39 ± 0.06	1.44 ± 0.10	1.29 ± 0.18
LVPW	1.33 ± 0.09	1.27 ± 0.11	1.37 ± 0.07	1.22 ± 0.12	1.27 ± 0.10	1.63 ± 0.32

Values are presented as mean ± SEM. EF ejection fraction; FS fractional shortening; LV left ventricular; ID inner diameter; AW anterior wall; PW posterior wall; student's t-test, $^{\#}p<0.05$, $^{\#\#}p<0.01$, $^{\#\#\#}p<0.001$ for iMgat1KO vs TCre groups at the same timepoint. N=8 Baseline and 14 dpi; N=6 TCre/5 iMgat1KO at 168 dpi.

Table S2 Summary of echocardiographic parameters comparing iMgat1KO mice to baseline measurements

Parameter			iMgat1KO			
Time	**Baseline**	**14 dpi**	**28 dpi**	**56 dpi**	**112 dpi**	**168 dpi**
Rate (BPM)	381 ± 21	410 ± 7	394 ± 9	399 ± 5	392 ± 6	370 ± 10
EF (%)	59.7 ± 0.8	59.0 ± 1.2	46.9 ± 1.7$^{\#\#\#}$	41.1 ± 1.5$^{\#\#\#}$	36.6 ± 0.8$^{\#\#\#}$	33.4 ± 1.7$^{\#\#\#}$
FS (%)	31.2 ± 0.5	31.1 ± 0.8	23.3 ± 1.0$^{\#\#\#}$	19.9 ± 0.9$^{\#\#\#}$	17.3 ± 0.4$^{\#\#\#}$	15.7 ± 0.9$^{\#\#\#}$
Diastole (mm)						
LVID	3.91 ± 0.28	4.33 ± 0.11	4.24 ± 0.090	4.12 ± 0.16	3.98 ± 0.10	3.53 ± 0.46
LVAW	0.84 ± 0.05	0.93 ± 0.04	1.00 ± 0.05$^{\#}$	1.10 ± 0.05$^{\#\#}$	1.07 ± 0.06$^{\#}$	1.07 ± 0.06$^{\#}$
LVPW	0.96 ± 0.08	0.86 ± 0.08	0.85 ± 0.05	0.99 ± 0.07	0.96 ± 0.07	1.80 ± 0.43
Systole (mm)						
LVID	2.58 ± 0.18	2.95 ± 0.10	3.28 ± 0.11$^{\#\#}$	3.45 ± 0.14$^{\#\#}$	3.34 ± 0.11	3.04 ± 0.33$^{\#\#}$
LVAW	1.39 ± 0.06	1.44 ± 0.10	1.35 ± 0.07	1.28 ± 0.08	1.27 ± 0.08	1.29 ± 0.18
LVPW	1.22 ± 0.12	1.27 ± 0.10	1.04 ± 0.06	1.10 ± 0.08	1.08 ± 0.08	1.63 ± 0.32

Values are presented as mean ± SEM. EF ejection fraction; FS fractional shortening; LV left ventricular; ID inner diameter; AW anterior wall; PW posterior wall; student's t-test, $^{\#}p<0.05$, $^{\#\#}p<0.01$, $^{\#\#\#}p<0.001$ for iMgat1KO vs baseline iMgat1KO measurements. N=8 Baseline through 56 dpi; N=5, 112 and 168 dpi.